



Wetting vs Droplet Aggregation: A Broadband Rotational Spectroscopic Study of 3-Methylcatechol...Water Clusters

Arsh S. Hazrah⁺, Aran Insausti⁺, Jiarui Ma, Mohamad H. Al-Jabiri, Wolfgang Jäger,* and Yunjie Xu*

Abstract: Two competing solvation pathways of 3-methylcatechol (MC), an atmospherically relevant aromatic molecule, with up to five water molecules were explored in detail by using a combination of broadband rotational spectroscopy and computational chemistry. Theoretically, two different pathways of solvation emerge: the commonly observed droplet pathway which involves preferential binding among the water molecules while the solute serves as an anchor point for the formation of a water cluster, and an unexpected wetting pathway which involves interactions between the water molecules and the aromatic face of MC, i.e., a wetting of the π -surface. Conclusive identification of the MC hydrate structures, and therefore the wetting pathway, was facilitated by rotational spectra of the parent MC hydrates and several H_2^{18}O and ^{13}C isotopologues which exhibit splittings associated with methyl internal rotation and/or water tunneling motions. Theoretical modelling and analyses offer insights into the tunneling and conversion barriers associated with the observed hydrate conformers and the nature of the non-covalent interactions involved in choosing the unusual wetting pathway.

Introduction

3-methylcatechol (MC), a benzene diol, plays an important role in atmospheric aerosol research. MC is a pyrolysis product of lignin, a major component of microfibrils in plant cells, which is released in significant amounts into the atmosphere during biomass burning. With its multiple hydrogen bond acceptor and donor sites, MC can readily bind with other atmospherically relevant molecules, such as water, organic acids, and sulfuric acid, to form atmospheric aerosol particles.^[1] Not only have studies of aerosol particles containing MC and its many oxidation products been reported,^[2] but MC has also often been selected as a representative congener of lignin pyrolysis products for investigations of ozonation pathways, influence of water contents, and ecotoxicity, both in laboratory experiments and theoretical modelling.^[2d,3] The detailed processes associated with the early phases of nucleation involving water, however, are still poorly understood. Relatedly, the presence of catalytic amounts of liquid additives, such as water, has been shown to facilitate nucleation and enhance crystallinity in the mechanochemical production of molecular crystals in most cases, whereas detrimental effects were reported in others,^[4] although very little is known about the mechanisms. Detailed knowledge of energetic and structural properties of small MC-water clusters is highly beneficial for the creation of benchmark data for modelling of aerosol particle formation. Of importance is, for example, how the conformational abundances and structures of the molecular target are modified by the addition of successive water molecules. Additionally, it would be of particular interest for theoretical benchmark studies to have explicit experimental data on how and at what point water molecules start to solvate the aromatic portion of a solute rather than pursue self-solvation, i.e., form a water droplet. Those insights are crucial in answering fundamental questions such as how many water molecules are needed to solvate an (organic) molecule.^[5]

The advent of chirp pulsed Fourier transform microwave (CP-FTMW) spectroscopy has provided a powerful tool to investigate the early phases of solvation by allowing one to easily and unambiguously track the sequential solvation one water molecule at a time. One recent highlight is the CP-FTMW study of microhydration of 3-methyl-3-oxentane-methano^[6] with one to six water molecules. The authors demonstrated convincingly that water molecules aggregate predominately with themselves, forming initially a one-dimensional chain and eventually three-dimensional

[*] Dr. A. S. Hazrah,⁺ Dr. A. Insausti,⁺ J. Ma, M. H. Al-Jabiri, Prof. Dr. W. Jäger, Prof. Dr. Y. Xu
 Department of Chemistry, University of Alberta
 Edmonton, AB T6G 2G2 (Canada)
 E-mail: wolfgang.jaeger@ualberta.ca
 yunjie.xu@ualberta.ca

Dr. A. S. Hazrah⁺
 Current Address: Department of Molecular Spectroscopy,
 Max Planck Institute for Polymer Research,
 Ackermannweg 10, 55128 Mainz, (Germany)

Dr. A. Insausti⁺
 Departamento de Química Física, Facultad de Ciencia y Tecnología,
 Universidad del País Vasco (UPV-EHU)
 48080 Bilbao (Spain)
 and
 Biofisika Institute (CSIC, UPV/EHU), University of the Basque
 Country (UPV/EHU)
 48940 Leioa (Spain)

[†] These authors contributed equally to this work.

© 2023 The Authors. Angewandte Chemie International Edition published by Wiley-VCH GmbH. This is an open access article under the terms of the Creative Commons Attribution Non-Commercial License, which permits use, distribution and reproduction in any medium, provided the original work is properly cited and is not used for commercial purposes.

cube-like geometries, leaving the hydrophobic parts of the molecule largely non-solvated.^[6] A similar pattern was observed in the fenchone-(H₂O)_{N=1-7} complexes.^[7] Interestingly, no water tunneling splittings were detected in any of these two microsolvation clusters.

MC, with its two OH functional groups, an aromatic ring and a methyl group, offers a unique opportunity to examine competing processes in solvating these different substituents, as well as the aromatic ring, in one molecule. Here, we report a CP-FTMW study of the solvation of MC with one to five water molecules in a stepwise fashion, with the aid of theoretical calculations. Our first significant finding is that a new solvation pathway, significantly distinct from the previously reported cases mentioned above, emerges. This not only highlights the intricate interplay between hydrophilic and hydrophobic solvation mechanisms, but also enhances our understanding of the solvation mechanism of aromatic systems. Second, both water tunneling and methyl internal rotation splittings were observed in several of the MC-(H₂O)_N clusters, offering a rare opportunity to gauge the solvation topology by following the evolution of the unique splitting patterns. Third, we emphasize the difference between experimentally observed conformers and theoretically predicted (local) minima and address the mismatches between them. Understanding the reasons for those discrepancies is of great importance in simulations of a range of molecular spectra observed in aqueous solution.^[8]

Results and Discussion

With its two neighbouring hydroxyl groups and its aromatic π -system, MC provides multiple and flexible hydrogen bonding opportunities, resulting in a complex conformational manifold of its small hydrates. To assist the spectroscopic assignments, the conformer-rotamer ensemble sampling tool CREST^[9] was utilized at the GFN2-xTB^[10] level to generate ensembles of mono-, di-, tri-, tetra-, and penta-hydrate conformations of MC. Further geometry optimizations and harmonic frequency calculations of the CREST candidates were carried out at the ω B97XD^[11]/Jun-cc-pVTZ^[12] level of theory. The theoretical methods and the theoretical conformational search results are summarized in Point S1, Supporting Information. In total, 16, 29, 100, 130, and 486 minimum energy structures were identified for the mono-, di-, tri-, tetra-, and penta-hydrates, respectively, at the DFT level. Very similar theoretical results were obtained at the B3LYP-D3BJ/def2-TZVP level of theory.

Using an energy window of 5 kJ mol⁻¹, the numbers of minima are reduced to 2, 3, 15, 21, and 9 for the mono-, di-, tri-, tetra-, and penta-hydrates respectively. We emphasize here the difference between a minimum and a conformer in the sense that a conformer can span multiple nearby minima which are connected by barrierless large amplitude motions (LAMs) (vide infra). The energetic and spectroscopic properties of the low energy minima within a 5 kJ mol⁻¹ energy window at the two different levels of theory are given in Tables S1.1–S1.2, and the complete listings are in Tables S1.3 and S1.4, SI. Each hydrate minimum, for

example MC1-1 W II, is named by the conformation of the monomeric subunit (MC1, see Figure S1.1, SI), number of water molecules (1 W), and energy ordering (II), with I being the most stable minimum for each hydrate. For conciseness, we refer exclusively to the ω B97XD results in the remaining text, unless specifically noted otherwise.

The rotational spectra of the hydrates of MC were measured using a CP-FTMW spectrometer, operating in the 2–6 GHz frequency range.^[13] A full description of the experimental details can be found in Point S2, SI. After removal of the known transitions belonging to the two main MC1 and MC2 monomeric conformers and their ¹³C isotopologues,^[14] some transitions with splitting patterns emerged. These were assigned to the six different hydrate species shown in Figure 1. The assignment of these species was based on the good agreement between the calculated and experimental rotational constants and the predicted trend of the energy ordering. The splitting patterns could be ascribed to methyl internal rotation components (1:1, A/E) and also to tunneling splittings associated with the exchange of identical hydrogen atoms of water (3:1, *ortho/para* spin statistics). It is fascinating to note how each hydrate species exhibits its own unique splitting pattern that depends on the specific solvation positions adopted by each water molecule (see Figure 1), a point we will further address below.

Generally, the A/E components of the methyl internal rotor were fit together using the XIAM program^[15] but the *ortho* and *para* species were fit separately. The species without visible splitting, i.e., MC2-1 W I, was fit using SPCAT/SPFIT.^[16] The resulting spectroscopic parameters (A-reduction, I' representation) of the six hydrated species are presented in Table 1. The spectroscopic analysis of the splitting patterns is briefly discussed below, while the details and the further analyses of the rare isotopologues are summarized in Point S3, SI, together with lists of rotational transition frequencies of all observed MC hydrates.

Below we address the crucial issue of unambiguously identifying the molecular carriers of the assigned sets of rotational transitions. Thanks to the high sensitivity of rotational spectroscopy to minor structural differences, one can often identify the corresponding molecular (heavy atom) frames based on the good agreement between the experimental and theoretical rotational constants, relative experimental versus theoretical intensities of *a*-, *b*- and *c*-type transitions, as well as the relative energy ordering of the theoretical conformer ensemble. Furthermore, the identification of the molecular carriers can be greatly supported by isotopic data.^[17] The spectroscopic evidences which support the general identification of each hydrate species shown in Figure 1 are elaborated below.

For the monohydrate, MC1-1 W I and MC2-1 W II were identified based firstly on the good agreement between the experimental and predicted rotational constants and the relative magnitude of the dipole moment components. Second, the global monohydrate minimum, MC1-1 W I, exhibits noticeable higher experimental intensity than MC2-1 W II. The detection of the much less stable MC2-1 W II can be explained by kinetic trapping in a jet expansion.^[18] The percentage abundance of the MC1 and MC2 monomers

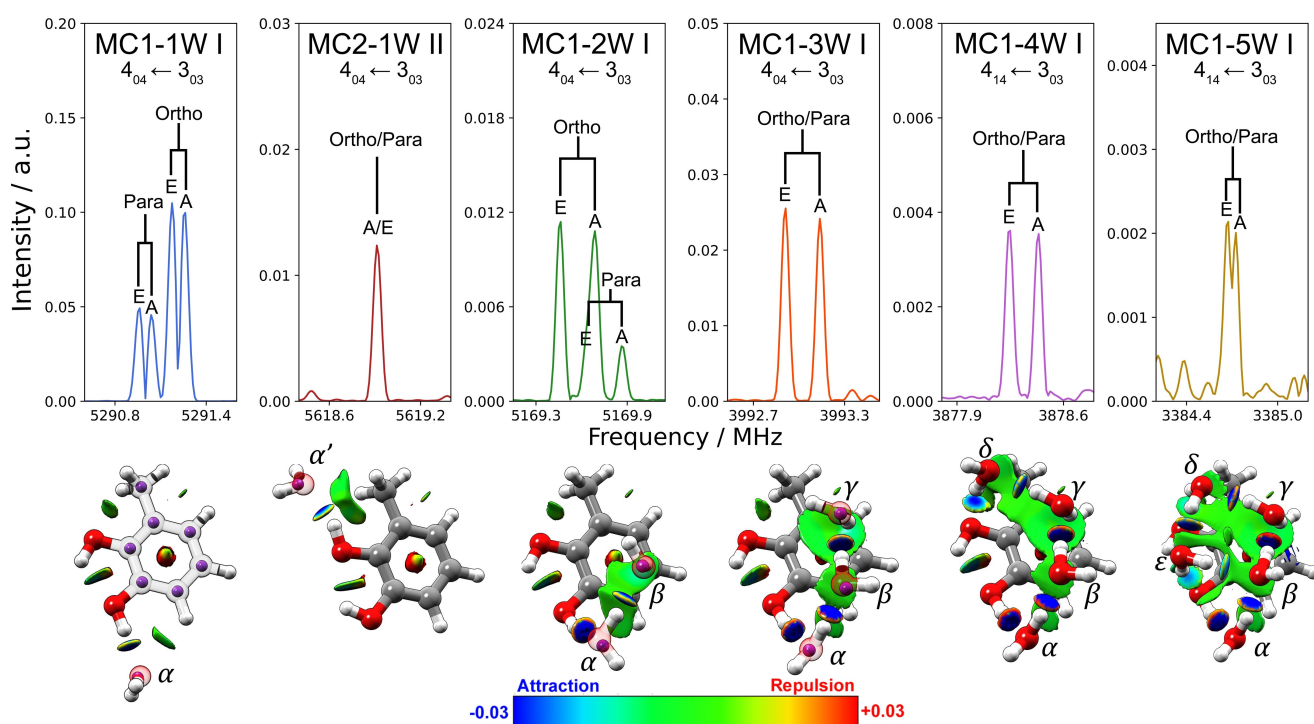


Figure 1. Top: Example transitions with characteristic tunneling splittings of the six hydrates assigned experimentally. Bottom: Optimized geometries of the six hydrates observed with the isosurfaces of the reduced electron density gradient from their NCI analyses. Blue (red) coloured surfaces represent attractive (repulsive) regions. The reduced electron density gradient was cut off at $s=0.7$ a.u. The successively solvating water molecules within the hydrates are labelled with Greek letters. The purple inner spheres represent the Kraitchman atom coordinates obtained using the rotational constants of respective singly substituted isotopologue species of MC-1 W to MC-3 W. Further discussion on hydrogen bond cooperative effects based on the theoretical, effective, and substitution structural details can be found in Point S3, SI.

Table 1: Spectroscopic parameters for the six experimentally assigned hydrates.

	MC1-1 W I		MC2-1 W II	MC1-2 W I		MC1-3 W I	MC1-4 W I	MC1-5 W I
	<i>ortho</i>	<i>para</i>		<i>ortho</i>	<i>Para</i>			
A/MHz	2284.10881(52)	2287.36875(76)	1857.482(14)	1381.2426(14)	1381.3352(19)	1081.07231(83)	783.98976(57)	674.82166(54)
B	779.65745(17)	779.59642(26)	908.21821(69)	714.13603(72)	714.14538(63)	539.95104(22)	481.04679(30)	443.58204(27)
C	585.24335(17)	585.17466(26)	616.02641(93)	606.38815(79)	606.41513(68)	472.49659(30)	448.19731(30)	395.04671(30)
Δ_J /kHz	0.0797(26)	0.0861(42)	0.123(17)	0.947(12)	0.999(16)	0.1429(35)	0.0666(44)	0.0555(34)
Δ_{JK}	0.404(11)	0.403(20)	[−0.1995]	−2.532(34)	−2.510(76)	[0.0576]	[0.0064]	[−0.0036]
Δ_K	[−0.3228] ^[a]	[−0.3228]	[1.0627]	3.987(63)	3.80(18)	0.292(31)	[0.0926]	[0.0302]
δ_j	[0.0179]	[0.0179]	[0.0287]	−0.0229(77)	[−0.0946]	[0.0127]	[−0.0022]	[0.0013]
δ_k	[0.3384]	[0.3384]	[0.2612]	[0.7601]	[0.7601]	[0.4299]	[0.2873]	[0.0781]
V_3 /kJ mol ^{−1}	3.50377(65)	3.50525(9)	N/A	3.5618(12)	3.54323(87)	3.3155(16)	3.4762(31)	3.5296(52)
ϵ /rad	[0.0] ^[a]	[0.0] ^[a]	N/A	[2.0114]	[2.0114]	1.390(48)	0.2005(98)	0.0207(48)
δ /rad	0.3675(19)	0.3633(28)	N/A	0.4767(23)	0.5144(17)	2.6619(35)	2.7630(88)	0.6577(79)
N	68	62	15	98	66	113	62	73
^[b] σ /kHz	2.6	3.7	4.9	11.1	11.6	6.5	5.7	6.4
^[c] $ \mu $ /D	$\mu_a > \mu_b$, no μ_c	$\mu_a > \mu_b$, no μ_c	μ_a , no μ_b or μ_c	$\mu_a > \mu_b > \mu_c$	$\mu_a > \mu_b > \mu_c$	$\mu_a \gg \mu_b > \mu_c$	$\mu_b > \mu_a$ no μ_c	$\mu_b > \mu_a$, no μ_c

^[a] Values in brackets are fixed to the theoretical ones. ^[b] Root-mean-square error of the fit. ^[c] Estimated relative magnitudes of dipole moment components.

in the jet was estimated to be about 60% and 40%, with an interconversion barrier of 13.2 kJ mol^{−1}, which limits the conformational conversion from MC2 to MC1.^[14] Interestingly, the addition of one water molecule noticeably increases the relative energy difference between MC2 and MC1 from 0.8 kJ mol^{−1} in the monomeric form to 4.6 kJ mol^{−1} in the monohydrate. These factors led to an

even higher abundance of MC1-1 W I versus MC2-1 W II compared to the monomers. The heavy atom positions were further verified by the analyses of one H₂¹⁸O and seven singly substituted ¹³C isotopologues of MC1-1 W I and one H₂¹⁸O isotopologue of MC2-1 W II (Point S3, SI).

Similarly, the molecular carriers of the di-, tri-, tetra- and pentahydrate were tentatively identified as MC1-2 W I,

MC1-3 W I, MC1-4 W I, MC1-5 W I, respectively based on the good agreement between the experimental and theoretical rotational constants, as well as the energetic ordering of the theoretical ensemble. For the dihydrate and trihydrate, the rotational spectra of the singly, doubly, and triply (trihydrate only) substituted ^{18}O water isotopologues could be assigned.

Using the experimental rotational constants of the H_2^{18}O and ^{13}C isotopologues, we performed Kraitchman's substitution analyses^[19] to obtain the O and C atom coordinates, and from those, the associated bond lengths and bond angles (see Table S3.1.3, SI) for the monohydrate up to the trihydrate. There is good agreement between the substitution structural parameters (r_s) and the structural parameters calculated at the $\omega\text{B97XD}/\text{Jun-cc-pVTZ}$ and $\text{B3LYP-D3-(BJ)}/\text{def2-TZVP}$ levels, where the differences are on average 1.8% and 1.3% for bond lengths and bond angles, respectively.

The observed characteristic tunneling splitting patterns are further evidence for the identification of the molecular carriers. For example, while MC1 exhibits methyl internal rotation splitting patterns with 1:1 intensity, MC2 does not,^[14] offering quick identification of transitions associated with MC1 or MC2. Using the nudged elastic band (NEB) procedure^[20] in ORCA 5.0.3^[21] and the synchronous transit quasi-Newton method^[22] in Gaussian 16, we identified the corresponding tunneling barriers and estimated the corresponding barrier heights at the $\omega\text{B97XD}/\text{Jun-cc-pVTZ}$ level (see Point S4, SI). The methyl internal rotation barrier heights (in kJ mol^{-1}) of the MC1-1 W I, -2 W I, -3 W I, -4 W I and -5 W I are calculated to be 3.5, 3.5, 3.3, 3.6, and 3.6 kJ mol^{-1} , respectively, in excellent agreement with the corresponding experimental (*ortho*) barrier heights of 3.5038(7), 3.562(1), 3.316(2), 3.476(2), and 3.530(5) kJ mol^{-1} .

To facilitate the water tunneling discussion, we label the successively solvating water molecules with Greek letters α (α'), β , γ , δ , and ϵ in Figure 1. The tunneling barrier for the exchange of two α protons in MC1-1 W I or two β protons in MC1-2 W I were calculated to be 3.5 and 3.7 kJ mol^{-1} , respectively. For MC2-1 W II and the tri-, tetra-, and pentahydrates, no proton exchange tunneling splittings were observed. For the trihydrate, the bonded α - and β -protons are locked into place by strong hydrogen bonding interactions, and the $\text{OH}\cdots\pi$ interaction between the bonded γ -proton and the π -surface of MC. This increases the tunnelling barrier to 7.2 kJ mol^{-1} which is sufficiently high to make the *ortho/para* doublet pattern unresolvable in our experiments. The same situation applies to the tetrahydrate and pentahydrate, where all protons of water are now locked into place by intermolecular interactions. Further discussions of the tunnelling barrier calculations for each hydrate are given in Point S4, SI.

Below we address two important challenges we encountered in identifying the observed hydrate conformers. Similar issues have been encountered in previous rotational spectroscopic studies of hydration clusters but have not been explored in great detail. First, based on the theoretical minima listed in Tables S1.1 and S1.2, one would expect to observe several conformers of dihydrate or tetrahydrate

experimentally, for example, rather than just one. Second, the relative experimentally derived magnitudes of the dipole moment components do not match the theoretical values well. For instance, the *a*- and *b*-type transitions of the observed MC1-2 W are of similar intensity and stronger than the *c*-type, whereas the $\mu_{a,b,c}$ values of MC1-2 W I are predicted to be 0.8, 1.9 and 0.7 Debye, respectively. This raises the question whether MC1-2 W I is the correct molecular carrier of the assigned transitions. Similar questions can be asked of the other larger hydrates shown in Figure 1.

For the hydrates, multiple minima are predicted,^[6,23] which have similar heavy atom molecular skeletons (i.e., similar rotational constants), but different free OH orientations, resulting in drastically different predicted dipole moment components. Often, these minima are also close in their relative energies. It has been increasingly recognized that multiple theoretical minima which differ only in their free OH orientations may correspond to only one stable conformer since the conformational conversion pathways among them become barrierless after zero-point energy corrections,^[24] thus complicating identification of the molecular carrier. In the MC1-2 W case, the first three minima, MC-2 W I to III, are within an energy window of $\approx 1 \text{ kJ mol}^{-1}$ and have the same heavy atom frame but different free OH pointing directions. Similar statements can be made for MC1-3 W I and II, MC1-4 W I to IV, and MC1-5 W. Here we use MC1-4 W as an example. As discussed in greater detail in Point S5, SI, the interconversion between I and II was modelled to be barrierless after ZPE correction, indicating that the experimentally observed tetrahydrate conformer takes on some character of both MC1-4 W I and II, as demonstrated before for some monohydrates.^[24b] In addition, the conversion barriers for III \rightarrow I and IV \rightarrow II are estimated to be on the order of 2 kJ mol^{-1} , implying efficient cooling of the higher energy local minima III and IV in the jet expansion. These calculations offer a reasonable explanation why only one MC1-4 W hydrate conformer was detected experimentally, even though many similarly low energy minima were predicted theoretically (Point S5, SI).

The experimental data and the associated theoretical modelling allowed us to confidently identify the six MC hydration frames given in Table 1 and Figure 1. We use the lowest energy minimum to name the observed conformer in each case, keeping in mind that other nearby minima (with the same heavy atom positions) which are connected by LAMs also contribute to some degree. The above discussion also provides rationale for the observation and non-observation of the predicted competitively low energy minima by invoking low barrier conformational cooling in a jet expansion and barrierless LAMs.

Importantly, the observed MC hydrates reveal an unusual preferred sequential solvation pathway which we denote as the *wetting* pathway. The process of "wetting" is defined here as the formation of more solvent-solute contacts with increasing number of solvent molecules while limiting the number of solvent-solvent interactions (see Figure 2). In previous microsolvation studies involving

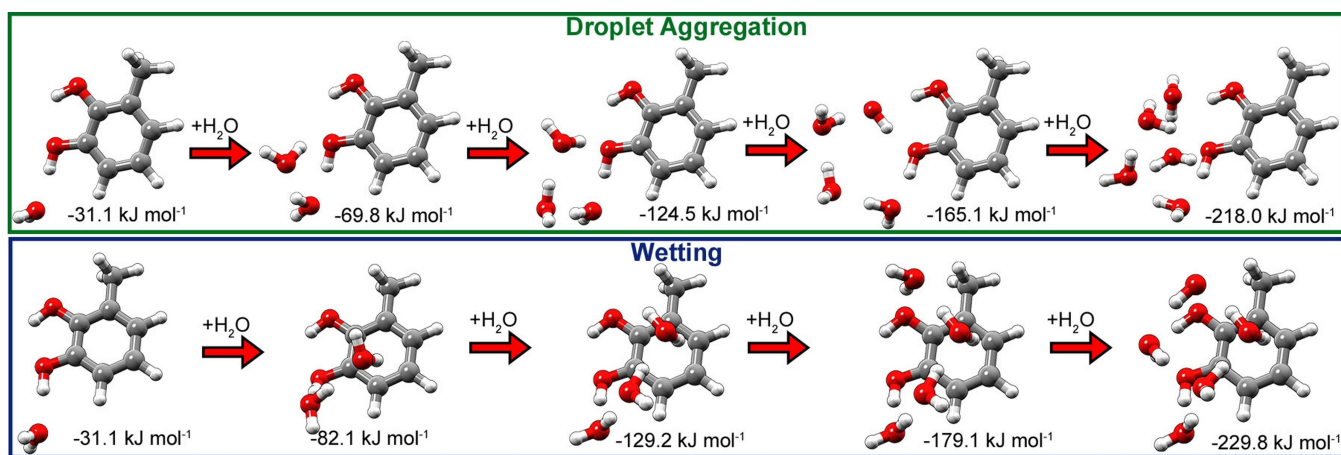


Figure 2. Two possible solvation pathways for MC based on the conformer searches and electronic structure calculations. The wetting pathway was observed experimentally. The counterpoise-corrected complexation energies are listed for each hydrate. See Point S7, Supporting Information for a more in-depth analysis of the intermolecular interactions.

systems with polar functional groups,^[25] a different solvation pathway is observed, i.e., *droplet aggregation*, where the water molecules preferentially bind among themselves to form a “droplet-like” water cluster. These “droplets” largely retain the structures of pure water clusters and the solute molecule provides an anchor point or anchor points for the “droplet” to form. Examples are the microsolvation studies of 3-methyl-3-oxetanemethanol,^[6] among others.^[26] The *droplet aggregation* pathway also dominates in the microsolvation of benzaldehyde^[27] where the cyclic water tetramer and pentamer retain similar structures as in the pure water cluster.^[28] From the calculated minimum energy structures in Table S1.1, SI, it is possible to construct solvation pathways of the *droplet aggregation* type; an example where pure water trimer through hexamer-like structures can be identified is shown in Figure 2. Included in Figure 2 are the counterpoise corrected complexation energies for the hydrate conformers associated with the two solvation pathways. Energetically, the *wetting* pathway shown is favoured over other, more conventional *droplet aggregation* pathways.

The results from non-covalent interactions (NCI)^[29] and quantum theory of atoms-in-molecules (QTAIM)^[30] analyses (see Point S6, Supporting Information for details) of the global hydrate minima associated with the five experimentally observed conformers are visualized in Figure 1 and Figure S6.2, respectively. The results for the minima involved in the *droplet aggregation* pathway are presented in Figure S6.1, SI. For the monohydrates, the QTAIM analyses show that the intermolecular interactions are dominated by a strong hydrogen bond interaction between a MC hydroxyl group and the water oxygen lone pair, with additional attractive $C_{\text{ring}}\text{H}\cdots\text{O}$ and $C_{\text{methyl}}\text{H}\cdots\text{O}$ interactions present in MC1-1 W I and MC2-1 W II, respectively. There is no visible interaction between the α or α' water with the aromatic ring of MC. For the dihydrate, the addition of the β water introduces a strong hydrogen bond interaction with the initial α water and also alters the interaction between the α water with MC. In the NCI plot, the second water molecule

begins to form a π -interaction “blanket” over the aromatic ring of MC. Already in the dihydrate a wetting of the aromatic part of MC begins, rather than formation of a self-aggregated cyclic structure with the hydroxyl group of MC (see Figure S6.1, SI). This preference is especially remarkable when considering the close proximity of two hydrogen bonding sites (i.e., the hydroxyl groups of MC) to the β -water molecule. This π -interaction is so strongly favoured that the ring OH is displaced by $\approx 38^\circ$ out of the ring plane compared to the MC1 monomer, to better accommodate the interaction of the two water molecules with the aromatic ring. In the trihydrate, the addition of the γ water continues to develop a chain-like structure to solvate the π face of MC. One could anticipate that in the tetrahydrate, the δ water molecule would finally begin to self-aggregate with the other three water molecules because of the limited aromatic surface of MC. To our surprise, the δ water molecule further extends the chain-like water structure to solvate the methyl group of MC, rather than induce a water self-aggregated structure (Figure S6.1, SI). At the pentahydrate, the MC ring is now fully saturated with water molecules, forcing the ϵ water to insert itself into the only available position: directly above the ring hydroxyl group while reducing the solvation of the δ water to the CH_3 group (Figure 1). The ϵ water molecule forms three canonical hydrogen bonds, two with the solvent, and one with the solute, not only extending the water chain, but also looping back to the initial part of the water chain. Overall, the MC hydrates in the *wetting* pathway exhibit substantial solvation of the whole MC molecule as highlighted by the green “blanket” of attractive interaction over the aromatic ring in the NCI plots, whereas those in the *droplet* pathway show water *droplet* formation driven by the hydrogen-bonding interactions among the OH groups of water and MC, with little to no interactions between the aromatic ring and water molecules. Similar to the previous studies,^[6,7,25–27] the MC hydrates in the *droplet* pathway contain water aggregates that show similarity to pure water clusters although with one OH of water replaced

by that of MC, with the 3D water-cluster like structure emerging in the MC pentahydrate (Figure 2). In contrast, the experimentally observed MC hydrates in the *wetting* pathway have drastically different water arrangements, emphasizing solvation of the aromatic face of MC.

Qualitatively, one may use the NCI plots in Figure 1 to justify the observation/non-observation of tunneling splittings in the observed transitions. Water tunneling splittings are observed in MC1-1 W I to MC1-2 W I and not in larger hydrates thanks to the increasing stronger π - and/or H-bond interactions involving the last added water molecule, i.e., α , β , γ , δ , and ϵ water in 1 W I to 5 W I, respectively. For MC2-1 W I, no water tunneling splitting was observed because of the close proximity of the H₂O and CH₃ groups. In terms of the methyl internal rotation, no methyl internal splitting was observed for MC2-1 W I, as in MC2.^[21] Interestingly, increasing water solvation in MC1-1 W I to MC1-5 W I has very minor effect on the methyl internal rotation barriers. This is because the additional solvation stabilizes both the ground state and the related transition state, leading to only minor changes in the difference. Also note that the actual magnitudes of the observed splittings depend on both the orientation of the methyl group in the molecule and the barrier height, and not on the barrier height alone.

Classically, different degrees of wetting can be ascribed to solid–liquid interfaces, which are quantified by the contact angle between the liquid–vapor interface and the solid–liquid interface.^[31] As it is difficult to borrow the contact angle concept directly for the MC hydrate clusters, one can perhaps define the degree of wettability based on the relative strength of solute (MC)–solvent (water) and water–water interactions in these clusters. Based on the NCI and QTAIM plots, these two families of interactions are both of similar strength, leading to a high degree of wettability when MC is solvated with water.

Conclusion

The preferred hydration pathway of MC was investigated in a step-by-step fashion, using rotational spectroscopy and several theoretical techniques. The systematic conformational CREST searches and the final geometry optimizations of MC with up to five water molecules generated a large number of low-energy hydrate minima. The rotational spectra of six mono- to pentahydrate conformers were analyzed in detail including the associated methyl internal rotation and water tunnelling splittings, as well as several H₂¹⁸O and ¹³C isotopologues. Comparison of the experimental rotational assignments of the parent and isotopic species with theory allowed us to confidently identify the heavy atom structures of the observed conformers. Furthermore, we successfully applied the NEB method to estimate the relevant conversion barriers to establish that an experimental conformer may contain contributions from multiple theoretical minima which are connected by barrierless LAMs. These insights from the gas phase hydration study are important since DFT minima of hydrate clusters are often used directly to simulate molecular spectra, such as

infrared and vibrational circular dichroism spectra, and such approaches may fail miserably when the minima are connected by barrierless motions and the observed ground state properties differ greatly from the predicted minima. The NEB results were also used to explain, by considering the cooling in a jet expansion, why only one hydrate conformer was detected for larger hydrates where many similarly low-energy minima were predicted. Extensive experimental data, coupled with theoretical analyses, conclusively demonstrate that the hydration of MC strongly prefers a *wetting* pathway, rather than the more commonly reported *droplet aggregation* microsolvation pathway. The NCI and QTAIM analyses as well as the splitting patterns of the methyl internal rotation and water tunnelling motions further corroborate the picture of a water-wetted aromatic ring surface.

Supporting Information

The authors have cited additional references within the Supporting Information.^[32–45]

Acknowledgements

This research was funded by the University of Alberta and the Natural Sciences and Engineering Research Council (NSERC) of Canada. We gratefully acknowledge access to the computing facilities by the Digital Research Alliance of Canada and Centro de Super Computación de Galicia (CESGA) from Spain. ASH and MHA acknowledge the support from H.E. Gunning Research Fellowships, Alberta Graduate Excellence Scholarships, and Marshall Syska Graduate Scholarships. AI's postdoctoral stay at the University of Alberta is partially funded by a fellowship from the Basque Government (Grant No. IT1491-22) and MCIN/AEI (Grant No. PID2020-117892RB-I00). YX is a Tier I Canada Research Chair in Chirality and Chirality Recognition.

Conflict of Interest

The authors declare no conflict of interest.

Data Availability Statement

The data that support the findings of this study are available in the supplementary material of this article.

Keywords: Hydration Clusters · Non-Covalent Interactions · Rotational Spectroscopy · Sequential Wetting · Tunneling Splitting

- [1] C. Coeur-Tourneur, A. Tomas, A. Guilloteau, F. Henry, F. Ledoux, N. Visez, V. Riffault, J. C. Wenger, Y. Bedjanian, *Atmos. Environ.* **2009**, *43*, 2360–2365.
- [2] a) M. S. Rana, M. I. Guzman, *Environ. Sci. Technol.* **2022**, *56*, 15437–15448; b) S. Frka, M. Sala, A. Kroflic, M. Hus, A. Cusak, I. Grgic, *Environ. Sci. Technol.* **2016**, *50*, 5526–5535; c) R. J. Mayorga, Z. Zhao, H. Zhang, *Atmos. Environ.* **2021**, *244*, 117910; d) D. Srivastava, T. V. Vu, S. Tong, Z. Shi, R. M. Harrison, *npj Clim. Atmos. Sci.* **2022**, *5*, 22; e) C. Coeur-Tourneur, V. Foulon, M. Laréal, *Atmos. Environ.* **2010**, *44*, 852–857.
- [3] J. Sun, B. Wei, Q. Mei, Z. An, X. Wang, M. He, *Chem. Eng. J.* **2019**, *358*, 456–466.
- [4] M. Arhangelskis, D.-K. Bučar, S. Bordignon, M. R. Chierotti, S. A. Stratford, D. Voinovich, W. Jones, D. Hasa, *Chem. Sci.* **2021**, *12*, 3264–3269.
- [5] A. Rognoni, R. Conte, M. Ceotto, *Chem. Sci.* **2021**, *12*, 2060–2064.
- [6] W. Sun, M. Schnell, *Angew. Chem. Int. Ed.* **2022**, *61*, e202210819.
- [7] a) M. Chrayteh, E. Burevschi, D. Loru, T. R. Huet, P. Dréan, M. E. Sanz, *Phys. Chem. Chem. Phys.* **2021**, *23*, 20686–20694; b) E. Burevschi, M. Chrayteh, D. Loru, P. Dréan, M. E. Sanz, *Int. Symp. on Mol. Spectrosc.*, June 20–24, 2022, Urbana, IL, U. S. A., <https://hdl.handle.net/2142/116891> **2022**.
- [8] a) K. Le Barbu-Debus, J. Bowles, S. Jähnigen, C. Clavaguéra, F. Calvo, R. Vuilleumier, A. Zehnacker, *Phys. Chem. Chem. Phys.* **2020**, *22*, 26047–26068; b) A. S. Perera, J. Thomas, M. R. Poopari, Y. Xu, *Front. Chem.* **2016**, *4*, 9; c) Y. Yang, J. Cheramy, M. Brehm, Y. Xu, *ChemPhysChem* **2022**, *23*, e202200161.
- [9] S. Grimme, C. Bannwarth, P. Shushkov, *J. Chem. Theory Comput.* **2017**, *13*, 1989–2009.
- [10] C. Bannwarth, S. Ehlert, S. Grimme, *J. Chem. Theory Comput.* **2019**, *15*, 1652–1671.
- [11] J.-D. Chai, M. H. Head-Gordon, *Phys. Chem. Chem. Phys.* **2008**, *10*, 6615–6620.
- [12] E. Papajak, J. Zheng, X. Xu, H. R. Leverentz, D. G. Truhlar, *J. Chem. Theory Comput.* **2011**, *7*, 3027–3034.
- [13] N. A. Seifert, J. Thomas, W. Jäger, Y. Xu, *Phys. Chem. Chem. Phys.* **2018**, *20*, 27630–27637.
- [14] A. S. Hazrah, M. H. Al-Jabiri, W. Jäger, *J. Mol. Spectrosc.* **2022**, *390*, 111715.
- [15] H. Hartwig, H. Dreizler, *Z. Naturforsch. A* **1996**, *51*, 923–932.
- [16] H. M. Pickett, *J. Mol. Spectrosc.* **1991**, *148*, 371–377.
- [17] F. Xie, M. Fusè, A. S. Hazrah, W. Jäger, V. Barone, Y. Xu, *Angew. Chem. Int. Ed.* **2020**, *59*, 22427–22430.
- [18] a) A. N. Mort, F. Xie, A. S. Hazrah, Y. Xu, *Phys. Chem. Chem. Phys.* **2023**, *25*, 16264–16272; b) A. Macario, S. Blanco, J. Thomas, Y. Xu, J. C. López, *Chem. Eur. J.* **2019**, *25*, 12325–12331; c) A. S. Hazrah, S. Nanayakkara, N. A. Seifert, E. Kraka, W. Jäger, *Phys. Chem. Chem. Phys.* **2022**, *24*, 3722–3732; d) A. S. Hazrah, M. Al-Jabiri, R. Speelman, W. Jäger, *Phys. Chem. Chem. Phys.* **2021**, *23*, 15159–15168.
- [19] J. Kraitchman, *Am. J. Phys.* **1953**, *21*, 17–24.
- [20] V. Ásgeirsson, B. O. Birgisson, R. Bjornsson, U. Becker, F. Neese, C. Riplinger, H. Jónsson, *J. Chem. Theory Comput.* **2021**, *17*, 4929–4945.
- [21] F. Neese, *Wiley Interdiscip. Rev.: Comput. Mol. Sci.* **2012**, *2*, 73–78.
- [22] C. Peng, H. Bernhard Schlegel, *Isr. J. Chem.* **1993**, *33*, 449–454.
- [23] J. Thomas, O. Sukhorukov, W. Jäger, Y. Xu, *Angew. Chem. Int. Ed.* **2014**, *53*, 7277–7280.
- [24] a) J. T. Gall, J. Thomas, F. Xie, Z. Wang, W. Jäger, Y. Xu, *Phys. Chem. Chem. Phys.* **2017**, *19*, 29508–29515; b) C. D. Carlson, A. S. Hazrah, D. Mason, Q. Yang, N. A. Seifert, Y. Xu, *J. Phys. Chem. A* **2022**, *126*, 7250–7260.
- [25] a) T. B. C. Vu, I. Kalkman, W. Leo Meerts, Y. N. Svartsov, C. Jacoby, M. Schmitt, *J. Chem. Phys.* **2008**, *128*, 214311; b) A. K. Huff, N. Love, K. R. Leopold, *J. Phys. Chem. A* **2021**, *125*, 8033–8046; c) B. Ouyang, T. G. Starkey, B. J. Howard, *J. Phys. Chem. A* **2007**, *111*, 6165–6175; d) W. Roth, M. Schmitt, C. Jacoby, D. Spangenberg, C. Janzen, K. Kleinermanns, *Chem. Phys.* **1998**, *239*, 1–9.
- [26] a) A. L. Steber, B. Temelso, Z. Kisiel, M. Schnell, C. Pérez, *Proc. Natl. Acad. Sci. USA* **2023**, *120*, e2214970120; b) S. Baweja, S. Panchagnula, M. E. Sanz, L. Evangelisti, C. Pérez, C. West, B. H. Pate, *J. Phys. Chem. Lett.* **2022**, *13*, 9510–9516.
- [27] W. Li, C. Pérez, A. L. Steber, M. Schnell, D. Lv, G. Wang, X. Zeng, M. Zhou, *J. Am. Chem. Soc.* **2023**, *145*, 4119–4128.
- [28] a) J. D. Cruzan, L. B. Braly, K. Liu, M. G. Brown, J. G. Loeser, R. J. Saykally, *Science* **1996**, *271*, 59–62; b) K. Liu, M. G. Brown, J. D. Cruzan, R. J. Saykally, *Science* **1996**, *271*, 62–64.
- [29] E. R. Johnson, S. Keinan, P. Mori-Sánchez, J. Contreras-García, A. J. Cohen, W. Yang, *J. Am. Chem. Soc.* **2010**, *132*, 6498–6506.
- [30] R. F. W. Bader, *Chem. Rev.* **1991**, *91*, 893–928.
- [31] D. Bonn, J. Eggers, J. Indekeu, J. Meunier, E. Rolley, *Rev. Mod. Phys.* **2009**, *81*, 739.
- [32] P. Pracht, E. Caldeweyher, S. Ehlert, S. Grimme, *Phys. Chem. Chem. Phys.* **2020**, *22*, 7169–7192.
- [33] T. Tsuneda, K. Hirao, *Wiley Interdiscip. Rev.: Comput. Mol. Sci.* **2014**, *4*, 375–390.
- [34] Z. Chen, Y. Li, Z. He, Y. Xu, W. Yu, *J. Chem. Res.* **2019**, *43*, 293–303.
- [35] M. J. Frisch, et al., *Gaussian 16, Revision C.01*, Gaussian, Inc., Wallingford, CT **2016**. See Supporting Information for the full reference.
- [36] AIMAll (Version 19.10.12), T. A. Keith, TK Gristmill Software, Overland Park KS, USA **2019** (aim.tkgristmill.com).
- [37] T. Lu, F. Chen, *J. Comput. Chem.* **2012**, *33*, 580–592.
- [38] F. Xie, N. A. Seifert, W. Jäger, Y. Xu, *Angew. Chem. Int. Ed.* **2020**, *59*, 15703–15710.
- [39] G. G. Brown, B. C. Dian, K. O. Douglass, S. M. Geyer, S. T. Shipman, B. H. Pate, *Rev. Sci. Instrum.* **2008**, *79*, 053103.
- [40] C. Pérez, S. Lobsiger, N. A. Seifert, D. P. Zaleski, B. Temelso, G. C. Shields, Z. Kisiel, B. H. Pate, *Chem. Phys. Lett.* **2013**, *571*, 1–15.
- [41] F. Xie, N. A. Seifert, M. Heger, J. Thomas, W. Jäger, Y. Xu, *Phys. Chem. Chem. Phys.* **2019**, *21*, 15408–15416.
- [42] N. Hansen, H. Mäder, T. Bruhn, *Mol. Phys.* **1999**, *97*, 587–595.
- [43] R. S. Ruoff, T. D. Klots, T. Emilsson, H. S. Gutowsky, *J. Chem. Phys.* **1990**, *93*, 3142–3150.
- [44] F. Weinhold, C. R. Landis, E. D. Glendening, *Int. Rev. Phys. Chem.* **2016**, *35*, 399–440.
- [45] E. D. Glendening, C. R. Landis, F. Weinhold, *J. Comput. Chem.* **2019**, *40*, 2234–2241.

Manuscript received: July 24, 2023

Accepted manuscript online: September 11, 2023

Version of record online: September 25, 2023